First-principles study of polyacetylene derivatives bearing nitroxide radicals

Beyza Bilgiç,[1] Çetin Kılıç,[1,*] and Burak Esat[2]

[1]*Department of Physics, Gebze Institute of Technology, Gebze, Kocaeli TR-41400, Turkey*
[2]*Department of Chemistry, Fatih University, Büyükçekmece, İstanbul TR-34500, Turkey*

Electrodes made of organic polymers bearing redox-active radical pendant groups have attractive features for use in rechargeable batteries. Electronic structure and electrochemical properties of cathode- and anode-active organic polymers are investigated here by means of first-principles calculations performed in the framework of the density functional theory. We consider organic radical polymers (ORPs) that consist of *trans*-polyacetylene derivatives bearing a variety of nitroxide radicals. A number of neutral and charged supercells are utilized to compute the ionization potentials and electron affinities as well as the one-electron states of these ORPs. By revealing the polyacetylene-derived highest occupied molecular orbital (HOMO) and lowest unoccupied molecular orbital (LUMO) as well as the radical-derived singly occupied molecular orbital (SOMO), the variation of the SOMO energy within the HOMO-LUMO gap is determined in the course of the oxidization or reduction of ORPs. Our results indicate that the ionization potential I and electron affinity A of polyacetylene would act as a lower or upper bound in the variation of the electrochemical potential of cathode- or anode-active ORPs in the course of battery discharge or charge owing to pinning of the radical-derived SOMO to the polyacetylene-derived HOMO or LUMO. Accordingly, it is anticipated that the electrochemical "window" $[-I, -A]$ of the polymeric backbone of ORPs will impose certain limitations in accomplishing a high charge/discharge voltage range in a totally organic rechargeable battery with positive and negative electrodes made of cathode- and anode-active ORPs, respectively. On the other hand, our findings suggest that one could, in principle, take advantage of using two different (conducting) polymeric backbones in the anode and cathode with adjusted HOMO and LUMO offsets *once* the electron transfer is accomplished to take place through the conducting backbones.

PACS number(s): 71.20.Rv, 82.45.Wx, 31.15.E−, 82.45.Fk

I. INTRODUCTION

Augmented usage of portable electronic devices in recent decades has been prompting researchers to design light, flexible, cost-effective, and nontoxic rechargeable batteries with enhanced charge/discharge rate capabilities.[1] Utilization of organic electrodes made of polymers bearing redox-active radical pendant groups has been proven[2,3] to be promising for satisfying these requirements. Organic electrodes made of radical polymers bearing pendant nitroxide (NO) groups have been employed as cathode-active materials (that exhibit *p*-type electrical conduction) in a variety of rechargeable batteries as surveyed in recent reviews.[4–6] On the other hand, the design of anode-active radical polymers turned out to be laborious.[7] Thus, there is a growing interest in the design of anode-active organic electrodes (that exhibit *n*-type electrical conduction). It should also be remarked that recent achievements[7–9] in designing anode-active organic electrodes have already made it possible to devise totally organic rechargeable batteries.

The operation of a battery containing a positive and/or negative electrode made of organic radical polymers (ORPs) relies on the oxidation and reduction characteristics of the utilized ORPs. From the perspective of the electronic structure, this parallels emptying or filling of the singly occupied molecular orbital (SOMO) of the ORP, which is normally populated by the unpaired electron of the pendant radical group. In this point of view, we investigate the electronic structure and electrochemical properties of cathode- and anode-active ORPs by performing first-principles calculations for *trans*-polyacetylene derivatives bearing a variety of nitroxide radicals. The molecular forms of the studied radical groups are given in Fig. 1. The radical with chemical formula $C_5H_6(NO)(CH_3)_4$

is 2,2,6,6-tetramethylpiperidin-1-oxyl (TEMPO), which has been used in the aforementioned studies,[2,3] and in combination with conducting polymers such as polyacetylene[10] and polythiophene,[11] producing a cathode-active electrode. The bipolar radical $C_6H_5–C_3(NO)_2(CH_3)_4$ includes two nitroxide groups and has very recently been utilized both in anode- and cathode-active fashion, yielding a poleless battery configuration.[9] The radical group $C_6H_4(CF_3)(NO)C(CH_3)_3$ has been designed,[8] via addition of the electron-withdrawing trifluoromethyl group, to produce an *n*-type radical polymer. In addition, we utilize a modified version of the latter given by the chemical formula $C_6H_4(CF_3)(NO)CH_3$ for the purpose of analysis and comparison. We discuss our results on *trans*-polyacetylene derivatives bearing these radical pendant groups in Sec. III, following a description of our computational modeling framework in Sec. II. We present a summary of the conclusions in Sec. IV, and disclose some technical (modeling) issues in Appendices A and B.

II. COMPUTATIONAL MODELING

In the modeling of the organic radical electrodes, viz., polyacetylene derivatives bearing nitroxide radicals, we employ first-principles total-energy and electronic-structure calculations based on the density functional theory (DFT) in combination with a number of (neutral and charged) supercells that contain a polymeric backbone bearing one of the aforementioned radical molecules. Atomistic structures contained in these supercells are all optimized, via minimization of the DFT-calculated total energy, as follows: First, the equilibrium structures are determined for the polymer backbone and the radical molecule in separate supercell calculations. The latter

$C_5H_6(NO)(CH_3)_4$ $C_6H_5-C_3(NO)_2(CH_3)_4$ $C_6H_4(CF_3)(NO)C(CH_3)_3$
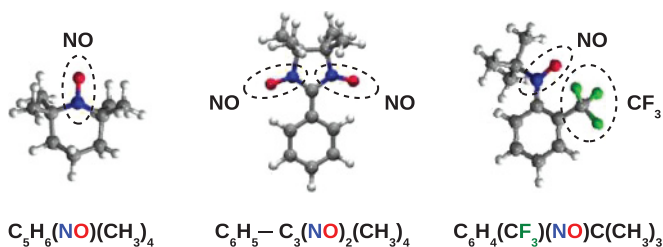
FIG. 1. (Color online) Nitroxide radicals that are attached to *trans*-polyacetylene in this study. The redox-active NO and electron-withdrawing CF_3 groups are marked.

two are then combined (with or without the aid of a "separator," i.e., some molecular unit put in between the two) within a (larger) supercell, and further relaxation of the combined structure is performed. This procedure is described in the upper panel of Fig. 2: First equilibrium structures for the polymeric backbone *trans*-$(CH)_{16}$ and the radical molecule (TEMPO) are individually determined. Polyacetylene and TEMPO are then combined with the aid of the separator COOH, and the combined structure is further relaxed to an equilibrium configuration. Note that the chemical formula for the resulting organic radical polymer is $C_{16}H_{15}-CO_2-C_5H_5(NO)(CH_3)_4$, i.e., a chemically sensible combination requires removal of one hydrogen from the polymer, one from the radical, and two from the separator.

The DFT-calculated total energies and other physical quantities reported here were obtained within the generalized gradient approximation (GGA) using the Perdew-Burke-Ernzerhof (PBE) exchange-correlation potential,[12] and employing the projector augmented-wave (PAW) method,[13] as implemented in VASP code.[14,15] The $1s^1$, $2s^2 2p^2$, $2s^2 2p^3$, $2s^2 2p^4$, and $2s^2 2p^5$ states are treated as valence states for hydrogen, carbon, nitrogen, oxygen, and fluorine, respectively. The plane-wave basis sets were determined by imposing a kinetic energy cutoff of 400 eV. An orthorhombic supercell with adequate dimensions was devised for each atomistic configuration, although supercells containing polymers bearing pendant groups were approximately cubic. A neutralizing
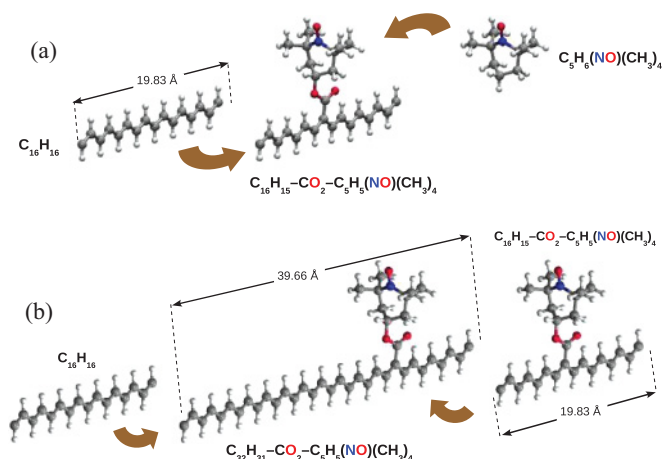
jellium background was employed for charged supercell calculations. The supercell dimensions were chosen to be fairly large (to include a vacuum region that put at least a distance of $\sim$20 Å between the repeating pendant groups in the neighboring supercells) in order to reduce image-charge interaction errors.[16] It was ensured that the supercell length along the polymeric axis was adequately large to cover many molecular units of *trans*-polyacetylene. In conjunction with this, only the Γ point was used for Brillouin zone sampling, viz., the band structure of one-dimensional crystal of *trans*-polyacetylene is virtually included through zone folding. It was, therefore, necessary to ensure the convergence of the total energy with respect to the supercell length L along the polymeric axis, i.e., the chain length of *trans*-polyacetylene. This analysis is presented in Appendix A.

In the optimization of the atomistic structure of the organic radical polymers, we used the chain of *trans*-$(CH)_{16}$ as the polymeric backbone that bears the radical pendant group, based on our analysis in Appendix A. This implies a distance of $\sim$20 Å between the pendant groups in neighboring supercells so that there is practically no interaction among the periodic images of the pendant group within the supercell geometry. We performed geometry optimizations for not only neutral, but also positively and negatively charged, configurations of the organic radical polymers, which are reported in Sec. III. For each supercell configuration, ionic relaxations were performed until the total energy is converged within 1 meV (resulting in a maximum value $\sim$0.002 eV/Å of residual forces on atoms).

Subsequent to geometry optimizations, we calculated the electronic structure, i.e., one-electron states, of the organic radical polymers and bare *trans*-polyacetylene. We performed analysis to assign the one-electron states either to the polymeric backbone or to the radical pendant group in order to reveal the variation of the polyacetylene-derived HOMO and LUMO state energies as well as the radical-derived SOMO state energy. The partial (state) charge densities were also obtained for the HOMO, SOMO, and LUMO states, which are presented in Sec. III. Concurrently, we computed the ionization potentials I and electron affinities A in order to elucidate the electrochemical characteristics of the studied *trans*-polyacetylene derivatives bearing nitroxide radicals. The latter are used to estimate the open cell voltage (OCV) for a number of *a priori* battery configurations (in which cathode- and anode-active ORPs are utilized as the positive and negative electrodes, respectively) thanks to the approximately linear correlations[17–19] between I (A) and the oxidation (reduction) potential. The ionization potential $I = E_{tot}(N_e - 1) - E_{tot}(N_e)$ and the electron affinity $A = E_{tot}(N_e) - E_{tot}(N_e + 1)$ are obtained using the total energy E_{tot} of neutral, negatively, and positively charged supercells containing N_e, $N_e + 1$, and $N_e - 1$ electrons, respectively. Encouraged by the convergence analysis presented in Appendix A, we used enlarged supercells in the calculations for I and A (as well as the HOMO, SOMO, and LUMO state energies), which contained *trans*-$(CH)_{32}$ as the polymeric backbone. These enlarged supercells were constructed by joining a bare *trans*-$(CH)_{16}$ chain to the *trans*-$(CH)_{16}$ chain bearing the pendant group, making the supercell length $\sim$40 Å, as demonstrated in Fig. 2(b). The supercell dimensions were actually doubled in all three directions so that

FIG. 2. (Color online) Construction of supercells containing polyacetylene derivative bearing TEMPO, which are employed for geometry optimizations (a) and electronic structure calculations (b).

the image-charge interaction error[16] was further reduced since the leading term in the image-charge correction is inversely proportional[16] to supercell length L. Therefore, we avoided using any image-charge correction schemes subject to debate in the literature,[20] and enlarged the supercells within the limits of our computational resources. It is also interesting to note that using the enlarged supercell with $trans$-$(CH)_{32}$ proves to be useful in obtaining the band gap from the total-energy differences as discussed in Appendix B, where we explore the relationship between the ionization potential (electron affinity) and HOMO (LUMO) energy for $trans$-polyacetylene.

III. RESULTS AND DISCUSSION

We consider ORPs formed by attaching the pendant groups CO_2–$C_5H_5(NO)(CH_3)_4$, C_6H_4–$C_3(NO)_2(CH_3)_4$, $C_6H_3(CF_3)(NO)C(CH_3)_3$, and $C_6H_3(CF_3)(NO)CH_3$ to $trans$-polyacetylene. Figure 3 shows the resulting atomistic structures for $C_{16}H_{15}$–CO_2–$C_5H_5(NO)(CH_3)_4$, $C_{16}H_{15}$–C_6H_4–$C_3(NO)_2(CH_3)_4$, $C_{16}H_{15}$–$C_6H_3(CF_3)(NO)C(CH_3)_3$, and $C_{16}H_{15}$–$C_6H_3(CF_3)(NO)CH_3$ obtained through the optimization process described in Sec. II. The optimized structures of the radical molecules and $trans$-polyacetylene as well as the values for the marked bond lengths d_{C-C} and d_{N-O} and bond angle θ_{C-C-C} are included for comparison. Comparative inspection of Figs. 3(a)–3(d) indicates significant structural changes in the polymeric backbone near the attachment point of the pendant group whereas it indicates rather slight modifications near the NO group. The charged configurations exhibit similar characteristics, as demonstrated in Fig. 4, where the bond lengths d_{N-O} and d_{C-C} are plotted as a function of the supercell charge. Note that the charged configurations for bare $trans$-polyacetylene and radical molecule are included for comparison. The upper graphs of Figs. 4(a)–4(d) show that both short and long C–C bonds near the attachment point in the combined system (of $trans$-polyacetylene derivative bearing radicals) are orderly longer than those of bare $trans$-polyacetylene. It is also seen that the C–C bond-length alternation (i.e., the difference between the long and short bond lengths) tends to diminish for highly charged (± 2) $trans$-polyacetylene, whereas it remains finite for $trans$-polyacetylene derivatives bearing radical groups. The lower graphs of Figs. 4(a)–4(d) show that the N–O bond length in the combined system (of $trans$-polyacetylene derivative bearing radicals) is almost the same as that in the radical molecule for neutral configurations, but it becomes congruously lower (higher) for positively charged (negatively charged) configurations. Thus, electron removal (cf. oxidation) from and electron addition (cf. reduction) to ORPs will produce shorter and longer N–O bonds in reference to the respective radical molecules. These differences confirm significant structural changes in the polymeric backbone near the attachment point, and signify rather pronounced modifications near the NO group in charged configurations. Thus, the oxidation or reduction of $trans$-polyacetylene derivatives bearing pendant radical groups would not be identical to that of either of its constituents. On the other hand, the analysis of the charge-density differences (not shown here) between the charged (± 1) and neutral configurations shows that the
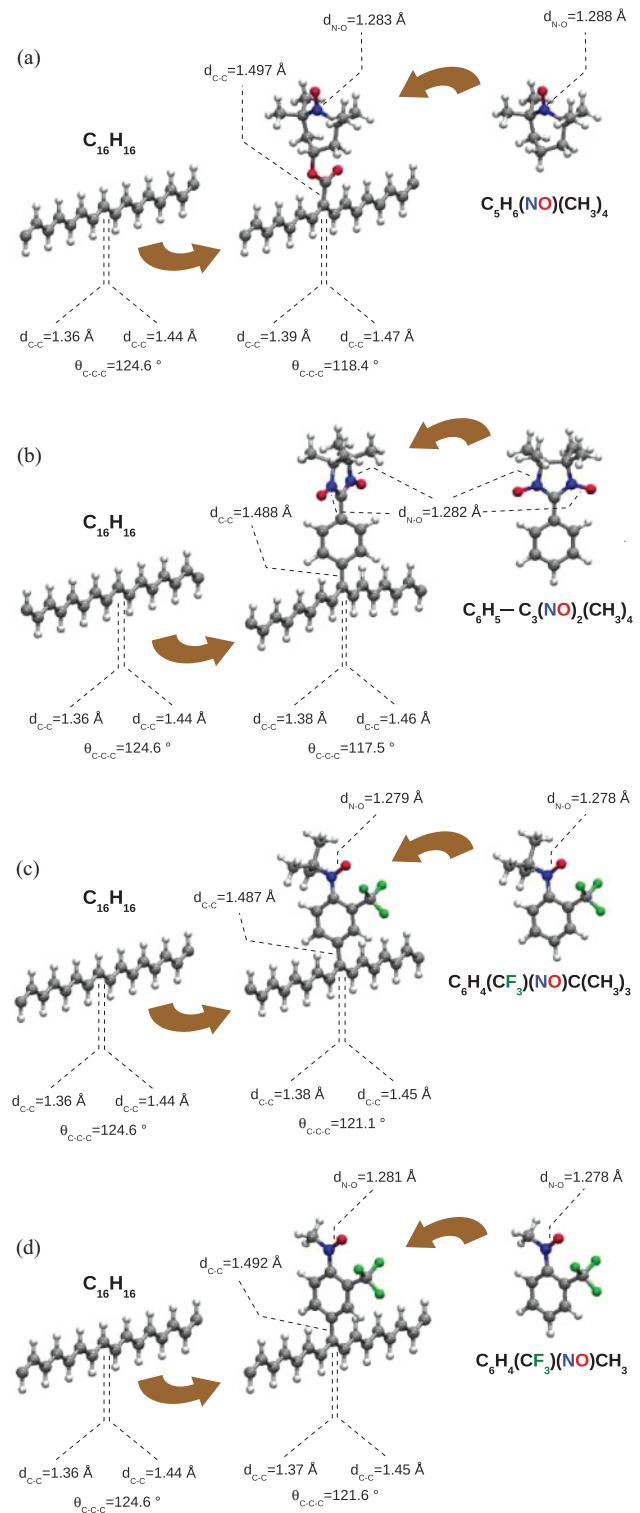
FIG. 3. (Color online) Optimized atomistic structures of $trans$-$(CH)_{16}$ derivatives bearing pendant groups CO_2–$C_5H_5(NO)(CH_3)_4$, C_6H_4–$C_3(NO)_2(CH_3)_4$, $C_6H_3(CF_3)(NO)C(CH_3)_3$, and $C_6H_3(CF_3)(NO)CH_3$, which are given in (a), (b), (c), and (d), respectively.

electron addition and withdrawal occurs mostly near the NO group, which is in line with the spatial localization of the SOMO state charge densities (given in Fig. 5 below).
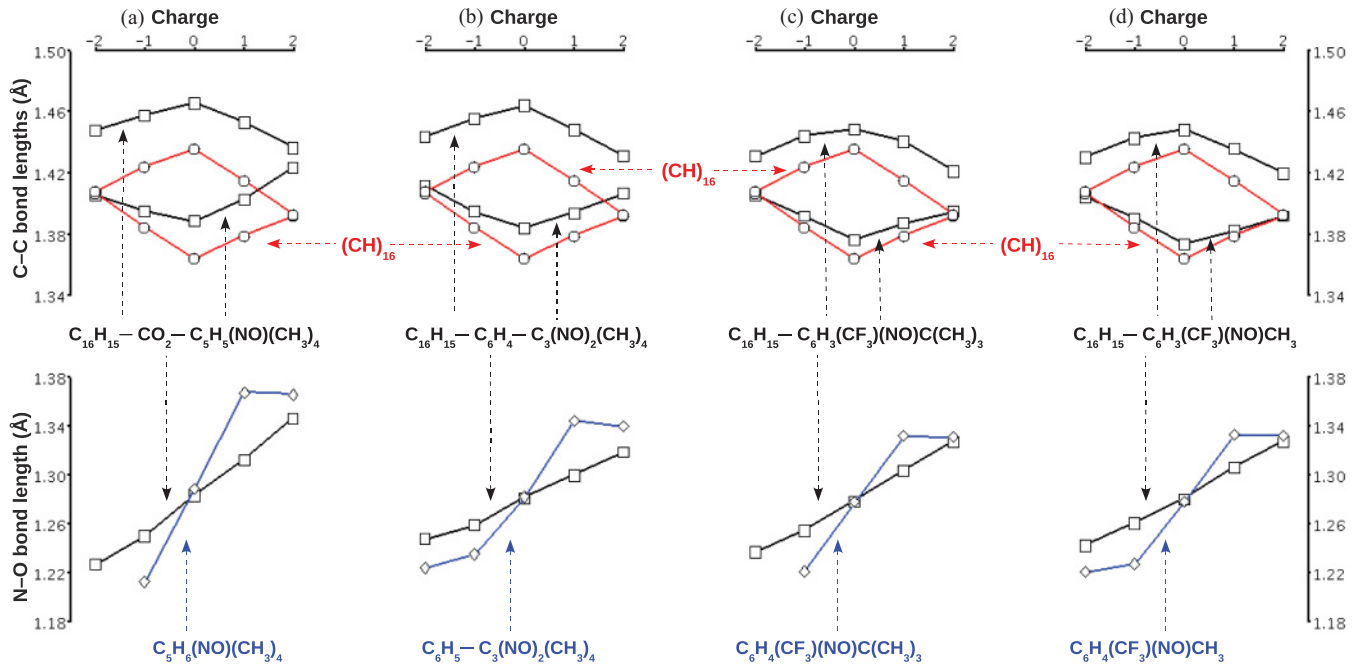
FIG. 4. (Color online) Variation of the optimized bond lengths d_{C-C} [upper graphs of (a)–(d)] and d_{N-C} [lower graphs of (a)–(d)] with the supercell charge q for *trans*-polyacetylene bearing pendant groups CO_2–$C_5H_5(NO)(CH_3)_4$, C_6H_4–$C_3(NO)_2(CH_3)_4$, $C_6H_3(CF_3)(NO)C(CH_3)_3$, and $C_6H_3(CF_3)(NO)CH_3$, which are given in (a), (b), (c), and (d), respectively. The C–C bond lengths for bare *trans*-$(CH)_{16}$ and the N–O bond length for the radical molecules are also included for comparison.

Hence, the oxidation or reduction is still restricted to the NO group in the *trans*-polyacetylene derivatives bearing radicals, with some delocalization reflecting the relaxation (owing to bonding to *trans*-polyacetylene) and charging effects.

Figure 5 shows the one-electron state energies (horizontal bars) for the neutral and charged ($q = \pm 1, 2$) *trans*-polyacetylene derivatives bearing nitroxide radicals and the isosurfaces representing the corresponding partial (state) charge densities. Analysis of the latter provides evidence in determining if a particular state is polymer or radical derived. In combination with this analysis, we utilize contributions from all atoms to the one-electron states in order to assign these states as (polyacetylene-derived) HOMO and LUMO or (radical-derived) SOMO. This procedure reveals that the states labeled as SOMO have ∼87%, 67%, and 93% contribution from the nitrogen and oxygen atoms of the NO group in the case of $C_{32}H_{31}$–CO_2–$C_5H_5(NO)(CH_3)_4$, $C_{32}H_{31}$–C_6H_4–$C_3(NO)_2(CH_3)_4$, and $C_{32}H_{31}$–$C_6H_3(CF_3)(NO)CH_3$, respectively. In accordance with this, the isosurfaces of the SOMO state charge densities are localized around the NO group as seen in Fig. 5. On the other hand, HOMO and LUMO have ∼93-98% contribution from the carbon and hydrogen atoms of the polyacetylene backbone. The visual resemblance of the state charge densities of the combined ORP system to those of $(CH)_{32}$ is an indicator for these characteristics. Having polyacetylene-derived HOMO and LUMO states determined, the one-electron energies are then shifted by an amount in accordance with setting the (polyacetylene) HOMO-LUMO midgap as *zero of energy* as seen in Fig. 5. This enables one to monitor the variation of SOMO state energy within the HOMO-LUMO gap in the course of the oxidization or

reduction of the radical polymers corresponding to electron removal ($q = +1$ or $+2$) from or addition ($q = -1$ or -2) to the supercells. It is seen that the SOMO energy of both *p*-type $C_{32}H_{31}$–CO_2–$C_5H_5(NO)(CH_3)_4$ and bipolar $C_{32}H_{31}$–C_6H_4–$C_3(NO)_2(CH_3)_4$ decreases and approaches the polyacetylene-derived HOMO in passing from the neutral configuration to the charged configuration with $q = +1$. If the supercell charge is further increased to $q = +2$, then the SOMO and HOMO energies turn out to be very close in value, as represented by almost indistinguishable (horizontal) bars in Fig. 5. Thus, the radical-derived SOMO state of a *p*-type organic radical polymer is pinned to the polyacetylene-derived HOMO state for a highly positively charged configuration. It is also noticeable in Fig. 5 that the SOMO energy of both *n*-type $C_{32}H_{31}$–CO_2–$C_5H_5(NO)(CH_3)_4$ and bipolar $C_{32}H_{31}$–C_6H_4–$C_3(NO)_2(CH_3)_4$ increases and approaches the polyacetylene-derived LUMO in passing from the neutral configuration to the charged configuration with $q = -1$. If the supercell charge is further increased to $q = -2$, then the SOMO and LUMO energies turn out to be very close in value, as represented by almost indistinguishable (horizontal) bars in Fig. 5. Thus, the radical-derived SOMO state of an *n*-type organic radical polymer is pinned to the polyacetylene-derived LUMO state for a highly negatively charged configuration. We note that these conclusions should extend to ORPs with a polymeric backbone longer than $C_{32}H_{31}$ because we obtained no significant change in the one-electron-state energies in a number of test calculations where $C_{32}H_{31}$ is replaced by $C_{48}H_{47}$.

If we consider a battery with electrodes made of the radical polymers included in Fig. 5, a highly charged configuration would occur when the *p*- and *n*-type electrodes are forced to
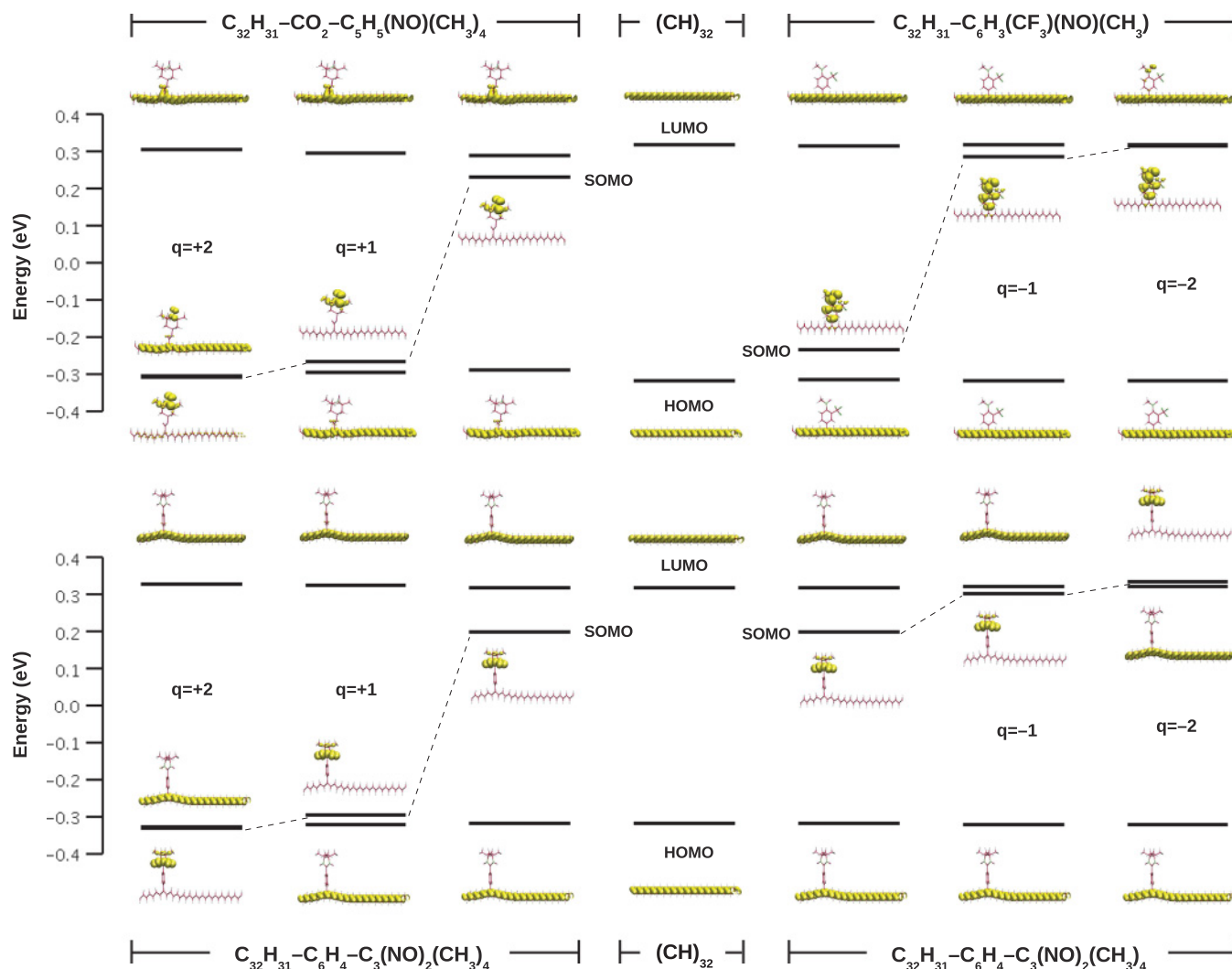
FIG. 5. (Color online) The one-electron (HOMO, SOMO, LUMO) state energies (horizontal bars) and the isosurfaces representing the state charge densities for the neutral and charged ($q = \pm 1, \pm 2$) *trans*-polyacetylene derivatives bearing nitroxide radicals.

become oxidized and reduced during battery charging with a rather high external voltage. In this situation, the radical-derived SOMO state of *p*- and *n*-type organic radical electrodes will be pinned to the polyacetylene-derived HOMO and LUMO states, respectively. Accordingly, the redox reactions cease to be restricted to the NO group and extend along the polymeric backbone. In this view, it is clear that the electrochemical "window" defined by the ionization potential and electron affinity (in other words, the band gap) of the polymeric backbone would impose certain limitations in terms of achieving a high charge/discharge voltage range with no stability issues. This situation resembles the case with the electrolyte "window" in Li batteries,[21] and points out the advantage of using a wide band gap or insulating polymer such as polyethylene[2] in making organic electrodes. It should be noted that the conducting polymers are rarely used[10,11] in the organic radical electrodes. On the other hand, a polymeric backbone of insulating nature has an important drawback in that it is necessary to incorporate conducting additives such as graphite into the electrode, which decreases the specific energy density of the battery cell.[3]

In order to complement the discussion (based on usage of the one-electron HOMO, LUMO, and SOMO energies) in the preceding paragraph, we present the ionization potentials and electron affinities of *p*- and *n*-type organic radical electrodes in Fig. 6. Note that pinning of the radical-derived SOMO state to the polyacetylene-derived HOMO (LUMO) state implies
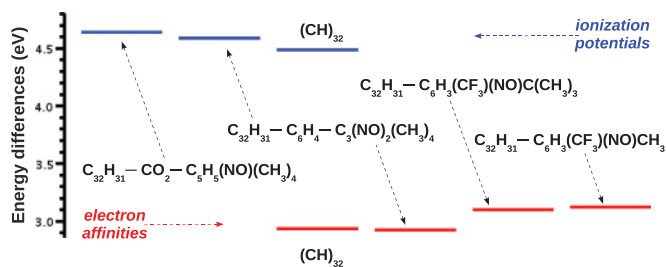
FIG. 6. (Color online) DFT-calculated ionization potentials and electron affinities (horizontal bars) of the cathode- and anode-active ORPs, respectively. Data for *trans*-$(CH)_{32}$ are also shown for comparison.

that $-I$ $(-A)$ would act as a lower (upper) bound in the variation of the electrochemical potential of cathode-active p-type (anode-active n-type) electrode in the course of battery discharge (charge). In Fig. 6, the ionization potential and electron affinity for *trans*-polyacetylene $(CH)_{32}$ are 4.49 eV and 2.93, respectively, which would agree with the asymptotic values obtained via extrapolation of DFT calculations[22] for the $(C_2H_2)_n$ oligomers with a finite chain length. Note that the calculated ionization potential (4.49 eV) falls in the lower end of the experimental value range[23,24] from 4.5 to 5.2 eV. Aside from this, as shown in Appendix B, the $I - A$ difference (1.55 eV) for *trans*-polyacetylene obtained from total-energy differences in a manner similar to the method of Chan and Ceder[25] implies only a slight overestimation in reference to the measured[17,23,26,27] band-gap values (1.4–1.5 eV), whereas the LUMO-HOMO one-electron energy difference expectedly[18,28] results in a large degree of underestimation. It is also worth noting that the calculated ionization potential difference ΔI between I of $C_{32}H_{31}$–CO_2–$C_5H_5(NO)(CH_3)_4$ and $C_{32}H_{32}$ is 0.15 eV in Fig. 6, which is on the same order of magnitude as the oxidation potential difference $\Delta E_{ox} = 0.28$ V estimated from the measured OCVs of the poly(2,2,6,6-tetramethylpiperidinyloxy-4-yl metacrylate)-lithium[2] and polyacetylene-lithium[17] batteries. Moreover, our calculations yield the $I - A$ difference of 1.66 eV for $C_{32}H_{31}$–C_6H_4–$C_3(NO)_2(CH_3)_4$, which agrees with the measured oxidation-reduction potential difference[29] and OCV of 1.33 V for the poleless battery[9] containing the cathode and anode, which are both made of radical polymers bearing C_6H_4–$C_3(NO)_2(CH_3)_4$ pendant groups.

Conjuring up totally organic batteries containing p- and n-type organic radical polymers included in Fig. 6 as the cathode and anode, respectively, we find that the OCV varies within $(E_g - 0.09, E_g + 0.16)$ V range, where E_g denotes the numeric value (1.55) of $I - A$ difference in eV for *trans*-polyacetylene. This finding is in line with the fact that $-I$ $(-A)$ of the polymeric backbone acts as a lower (upper) bound in the variation of the electrochemical potential of p-type (n-type) electrode in the course of battery discharge (charge) owing to pinning of the radical-derived SOMO state to the polymer-derived HOMO (LUMO) state. Assuming that this behavior is not restricted to polyacetylene so that it can be generalized to other low-band-gap polymers, one might hope to achieve a higher OCV by using two different conducting polymers on the cathode and anode with tailored "band offsets" between HOMO and LUMO levels, i.e., the location of electrochemical windows, of the polymeric backbones. It should, however, be noted that the electron transfer through the polymeric backbone appears not to play an essential role in the working mechanism of the organic radical electrodes produced to date.[6,30] So, one must first fulfill the electron transfer through the (conducting) polymeric backbone in order to exploit tailoring of the electrochemical window.

IV. CONCLUSION

In summary, our first-principles approach provides a means to monitor the variation of electronic structure, viz. polyacetylene-derived HOMO and LUMO and radical-derived SOMO state energies, in the course of oxidation and reduction of cathode- and anode-active *trans*-polyacetylene derivatives bearing a variety of nitroxide radicals. Our results indicate that the redox reactions would take place around the NO group with some delocalization reflecting the relaxation (owing to bonding to *trans*-polyacetylene) and charging effects. We find that the radical-derived SOMO state of cathode-active (anode-active) organic radical polymer is pinned to the polyacetylene-derived HOMO (LUMO) state for a highly charged configuration. Thus, the electrochemical window of the polymeric backbone imposes certain limitations in accomplishing a high charge/discharge voltage range with no stability issues. Our findings suggest that one could, in principle, take advantage of using two different (conducting) polymeric backbones in the anode and cathode with tailored band offsets provided that the electron transfer is engineered to take place through the polymeric backbone.

APPENDIX A: CONVERGENCE WITH RESPECT TO CHAIN LENGTH OF *trans*-POLYACETYLENE

It was noted[31–33] that a dense **k**-point sampling of the Brillouin zone was crucial for the energy convergence when the primitive unit cell of the one-dimensional crystal of *trans*-polyacetylene was employed in the calculations. Recent studies,[34,35] however, reveal that Brillouin zone sampling by ~16 **k** points yields reasonable accuracy. Using the Γ point of the Brillouin zone of the supercell that contains *trans*-$(CH)_x$ is equivalent to using $x/2$ **k** points of the unfolded Brillouin zone. It is, therefore, imperative for us to study the convergence of the total energy with respect to the chain length of *trans*-polyacetylene, viz., the supercell length L along the polymeric axis. Thus, we performed a series of calculations employing a variety of supercells with increasing L_x containing $x = 4, 8, 16, 32$, or 48 CH units. We define a lattice parameter $a_x = L_x/x$ specific to each supercell, which is comparable to the lattice parameter a of the primitive unit cell of the one-dimensional crystal of *trans*-polyacetylene. Note that L_x, a_x, and a would be all identical for $x = 1$ (when the supercell is devised to be the same as the primitive unit cell of the one-dimensional crystal of *trans*-polyacetylene). The equilibrium value of a_x corresponds to the optimized geometry of *trans*-$(CH)_x$ within the supercell with length L_x. Thus, for each supercell configuration, ionic relaxations are performed until the total energy is converged within 1 meV. The curves in Fig. 7(a) are obtained via this procedure, showing the energy per molecular unit E_x as a function of a_x. Note that equilibrium values for E_x and a_x correspond to the minima of these curves. It is seen that the curves for $x = 48$, $x = 32$, and $x = 16$ are visually almost identical, indicating that the supercell containing *trans*-$(CH)_x$ with $x \geqslant 16$ is sufficiently large in regard to the energy convergence. The latter could also be inferred by inspecting the curve in Fig. 7(b), which represents the equilibrium value of E_x as a function of the supercell length L_x. For the sake of quantitative analysis, we have $E_{16} - E_{48} = 27$ meV and $E_{32} - E_{48} = 4$ meV in Fig. 7.
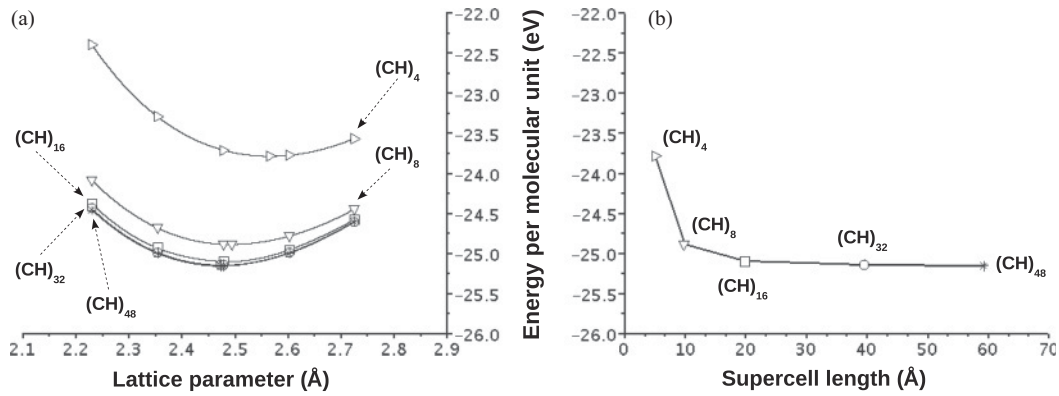
FIG. 7. Binding-energy curves (a) for *trans*-$(CH)_x$ with $x = 4, 8, 16, 32$, or 48 and the energy per molecular unit as a function of the length of the corresponding supercells (b).

Thus, the variation of the energy (per CH unit) with x would be smaller than 4 and 27 meV for $x \geqslant 32$ and 16, respectively. Accordingly, *trans*-$(CH)_{32}$ [as opposed to *trans*-$(CH)_{16}$] was used to compute the total-energy differences I and A in Sec. III.

It turns out that the DFT-optimized values for short and long C–C bond lengths are the same as the experimental values[36] (of 1.36 and 1.44 Å, respectively) for $x = 16$, i.e., for *trans*-$(CH)_{16}$ corresponding to equilibrium value of $L_{16} = 19.83$ Å. On the other hand, the C–C–C bond angle (cf. Fig. 3) is slightly overestimated in reference to the experimental value of 122°; but, the present value is indeed in agreement with the reported DFT-optimized values.[15] We should also note that the bond-length alternation (BLA), i.e., the difference between the long and short bond lengths, is reduced as the length of the *trans*-$(CH)_x$ chain increases. This behavior, i.e., the variation of the short and long C–C bond lengths with the supercell length L_x, is shown in in Fig. 8(a). The calculated BLA becomes significantly smaller than the measured[36] BLA (0.08 Å) as the chain length of *trans*-$(CH)_x$ approaches infinity. This finding is in line with the previous DFT and *ab initio* calculation results.[15,18,33–35,37] This problem of underestimation of BLA has been remarked by various groups,[33–35,37] the resolution of which is beyond the scope of this paper because it would require improvement in the description of the exchange-correlation potential.[18,37,38] Since the short and long bond lengths (cf. BLA) obtained with the supercell length $L_{16} = 19.83$ Å coincides with the measured values, *trans*-$(CH)_{16}$ was employed as the polymeric backbone in geometry optimizations described in Sec. II.

It is known[37,39] that the bond-length alternation and the band gap of *trans*-polyacetylene are related. Thus, we present the variation of the HOMO and LUMO energies with the supercell length in Fig. 8(b). It is seen that the variation of the HOMO and LUMO energies with x is on the order of 150 meV for $x \geqslant 16$ but less than 40 meV for $x \geqslant 32$. Thus, *trans*-$(CH)_{32}$ [as opposed to *trans*-$(CH)_{16}$] was employed as the backbone of ORPs in Section III. It is also seen, in Fig. 8(b), that the HOMO-LUMO gap is reduced as the supercell length approaches infinity, yielding a value much smaller than the measured[17,23,26,27] value range of 1.4–1.5 eV. This is related to underestimation of BLA since the HOMO-LUMO gap [cf. Fig. 8(b)] and BLA [cf. Fig. 8(a)] are linearly correlated

according to the following relationship (obtained via fitting): HOMO-LUMO gap = 8.135 BLA + 0.030 eV, where BLA is in Å. Underestimation of the gap is also originated[18,28] from derivative discontinuities[40,41] of the exchange-correlation
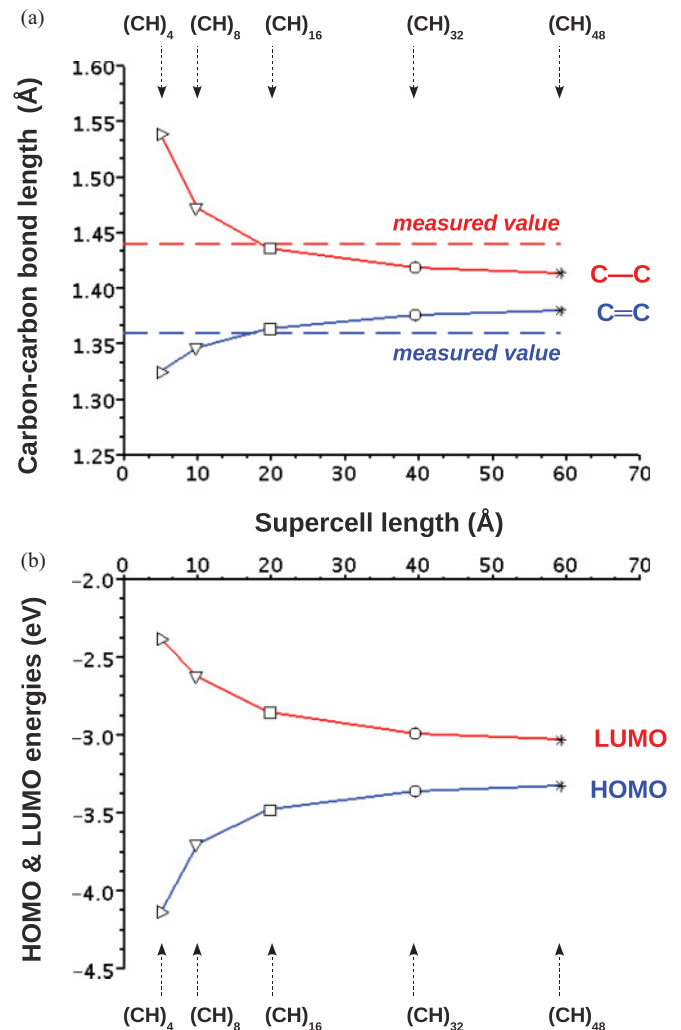
FIG. 8. (Color online) The DFT-optimized C–C bond length (a) and DFT-calculated HOMO and LUMO energies (b) as a function of the length of supercells containing *trans*-$(CH)_x$ with $x = 4, 8, 16, 32$, or 48.
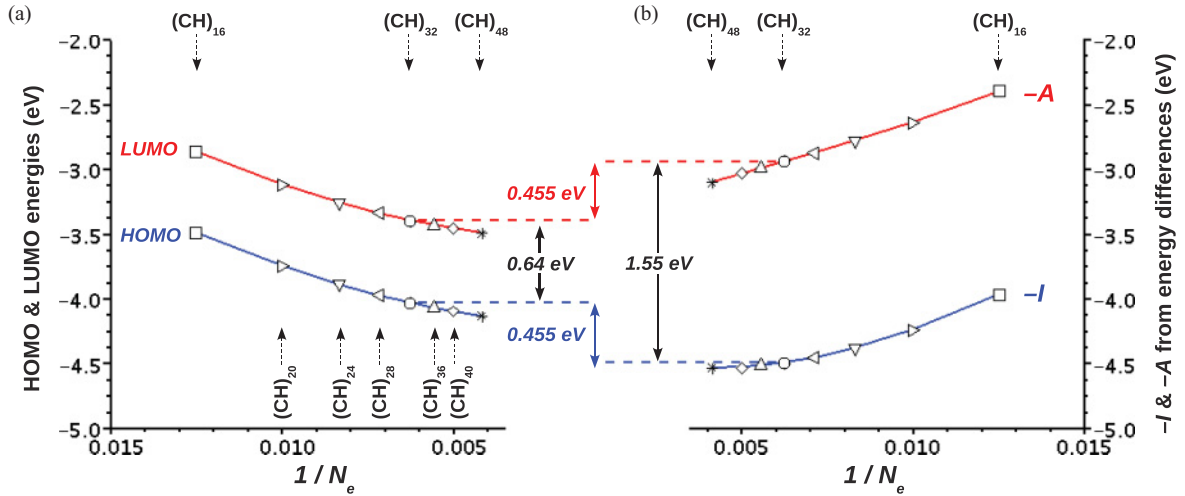
FIG. 9. (Color online) The ionization potential I and electron affinity A (b) and the HOMO and LUMO energies ϵ_v and ϵ_c (a) as a function of the ratio of the number of electrons added to (or removed from) the (neutral) supercell to the total number of electrons N_e.

energy and/or the delocalization error[42] within DFT-GGA, which precludes a sensible comparison of calculated and measured values of the band gap. Thus, we utilize an alternative approach described in Appendix B in order to estimate the band gap, which is based on usage of the total-energy differences in a manner similar to the method of Chan and Ceder.[25]

APPENDIX B: RELATIONSHIP BETWEEN THE IONIZATION POTENTIAL (ELECTRON AFFINITY) AND HOMO (LUMO) ENERGY

The relationship between the difference $I - A$ and the band gap obtained from the Kohn-Sham eigenvalues can be expressed as follows:

$$I - A = \epsilon_c - \epsilon_v + \Delta, \tag{B1}$$

where ϵ_c and ϵ_v denote the one-electron (LUMO and HOMO) orbital energies, and Δ is a constant reflecting the derivative discontinuity[40,41] of the exchange-correlation energy and the delocalization error.[42] Thus, we compare the ionization potential and electron affinity (I and A) with the HOMO and LUMO energies (ϵ_v and ϵ_c) for a series of supercells with increasing length of *trans*-$(CH)_x$ with $x = 16, 20, 24, 28, 32, 36, 40,$ or 48, in Fig. 9: Figures 9(a) and 9(b) shows I and A [ϵ_v and ϵ_c] as a function of the ratio $1/N_e$ of the number of electrons added to (or removed from) the (neutral) supercell to the number of electrons N_e of the neutral supercell. Both $-I$ and $-A$ decrease as $1/N_e$ decreases, i.e., x increases. The difference $I - A$ also exhibits a decreasing variation for $1/N_e < 0.01$ (i.e., $x > 20$), as seen more clearly in Fig. 10. Since the delocalization error[42] would get enhanced as x increases, we think that there is an optimum value of x corresponding to the most reliable value of the predicted band gap $I - A$. This consideration is evidenced by the fact that the delocalization error[42] could significantly be reduced[25] by using one electron per screening volume in the computation of the total energies of the charged configurations, which are used to predict the band gap.

We employed the supercells containing *trans*-$(CH)_{32}$ as the polymeric backbone in the electronic structure calculations, as described in Sec. II. This choice, viz., $x = 32$, resulted in a reasonable value for I of *trans*-polyacetylene as discussed in Sec. III. We see in Fig. 9 that the band gap is $I - A = 1.55$ eV for $x = 32$, which implies only a slight overestimation in reference to the measured[17,23,26,27] band-gap values (1.4–1.5 eV), and is smaller than electronic excitation energy[24] of 1.9 eV. On the other hand, $\epsilon_c - \epsilon_v$ difference (0.64 eV) expectedly[18,28] results in a large degree of underestimation.

In the calculations yielding the curves given in Fig. 9, the geometry of the *trans*-$(CH)_x$ was fixed to be that of *trans*-$(CH)_{16}$ so that the number of molecular units and the supercell length were increased without performing ionic relaxations. Thus, the $\epsilon_c - \epsilon_v$ difference remains approximately constant, whereas the $I - A$ difference varies while $1/N_e \rightarrow 0$, as seen more clearly in Fig. 10. Therefore, Δ follows the variation of
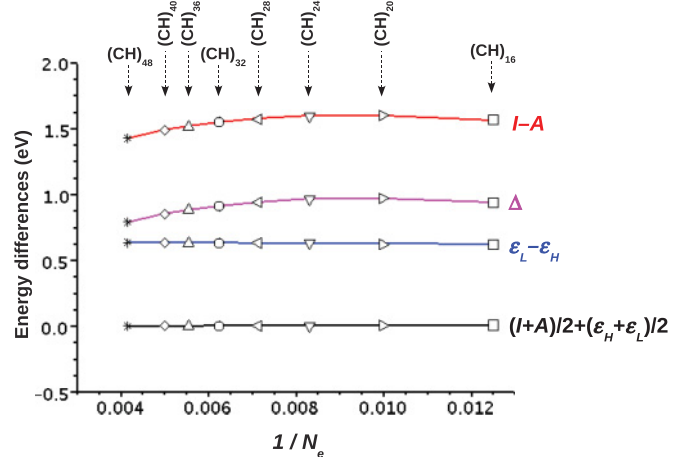
FIG. 10. (Color online) The band-gap-related differences $I - A$ and $\epsilon_c - \epsilon_v$ as a function of the ratio of the number of electrons added to (or removed from) the (neutral) supercell to the total number of electrons N_e.

$I - A$ since $\Delta = (I - A) - (\epsilon_c - \epsilon_v)$. It is also clear from Fig. 10 that the band center $-(I + A)/2$ obtained from the total-energy differences and the band center $(\epsilon_v + \epsilon_c)/2$ obtained from one-electron orbital energies remain equal regardless of the value of N_e, or in other words x, as expected (cf. Ref. 40).

---

*Corresponding author: cetin_kilic@gyte.edu.tr

[1] H. Nishide and K. Oyaizu, Science **319**, 737 (2008).

[2] K. Nakahara, S. Iwasa, M. Satoh, Y. Morioka, J. Iriyama, M. Suguro, and E. Hasegawa, Chem. Phys. Lett. **359**, 1165 (2002); H. Nishide, S. Iwasa, Y.-J. Pu, T. Suga, K. Nakahara, and M. Satoh, Electrochim. Acta **50**, 827 (2004).

[3] K. Nakahara, J. Iriyama, S. Iwasa, M. Suguro, M. Satoh, and E. J. Cairns, J. Power Sources **163**, 1110 (2007).

[4] H. Nishide and T. Suga, Electrochem. Soc. Interface **14**, 32 (2005).

[5] A. K. Shukla and T. P. Kumar, Curr. Sci. **94**, 314 (2008).

[6] K. Nakahara, K. Oyaizu, and H. Nishide, Chem. Lett. **40**, 222 (2011).

[7] T. Suga, H. Ohshiro, S. Sugita, K. Oyaizu, and H. Nishide, Adv. Mater. **21**, 1627 (2009).

[8] T. Suga, Y.-J. Pu, S. Kasatori, and H. Nishide, Macromolecules **40**, 3167 (2007).

[9] T. Suga, S. Sugita, H. Ohshiro, K. Oyaizu, and H. Nishide, Adv. Mater. **23**, 751 (2011).

[10] T. Katsumata, M. Satoh, J. Wada, M. Shiotsuki, F. Sanda, and T. Masuda, Macromol. Rapid Commun. **27**, 1206 (2006); J. Qu, T. Katsumata, M. Satoh, J. Wada, J. Igarashi, K. Mizoguchi, and T. Masuda, Chem.– Eur. J. **13**, 7965 (2007).

[11] M. Aydin, B. Esat, Ç. Kılıç, M. E. Köse, A. Ata, and F. Yılmaz (unpublished) .

[12] J. P. Perdew, K. Burke, and M. Ernzerhof, Phys. Rev. Lett. **77**, 3865 (1996).

[13] P. E. Blöchl, Phys. Rev. B **50**, 17953 (1994).

[14] G. Kresse and J. Furthmüller, Phys. Rev. B **54**, 11169 (1996).

[15] G. Sun, J. Kürti, P. Rajczy, M. Kertesz, J. Hafner, and G. Kresse, J. Mol. Struct., THEOCHEM **624**, 37 (2003).

[16] G. Makov and M. C. Payne, Phys. Rev. B **51**, 4014 (1995).

[17] J. L. Brédas, R. Silbey, D. S. Boudreaux, and R. R. Chance, J. Am. Chem. Soc. **105**, 6555 (1983).

[18] S. Yang, P. Olishevski, and M. Kertesz, Synth. Met. **141**, 171 (2004).

[19] R. S. Ruoff, K. M. Kadish, P. Boulas, and E. C. M. Chen, J. Phys. Chem. **99**, 8843 (1995); S. Janietz, D. D. C. Bradley, M. Grell, C. Giebeler, M. Inbasekaran, and E. P. Woo, Appl. Phys. Lett. **73**, 2453 (1998); M. Yoshimura, K. Honda, T. Kondo, R. Uchikado, Y. Einaga, T. N. Rao, D. A. Tryk, and A. Fujishima, Diamond Relat. Mater. **11**, 67 (2002); X. Wu, A. P. Davis, P. C. Lambert, L. K. Steffen, O. Toy, and A. J. Fry, Tetrahedron **65**, 2408 (2009).

[20] I. Dabo, B. Kozinsky, N. E. Singh-Miller, and N. Marzari, Phys. Rev. B **77**, 115139 (2008); N. D. M. Hine, K. Frensch, W. M. C. Foulkes, and M. W. Finnis, *ibid.* **79**, 024112 (2009); S. Lany and A. Zunger, Modelling Simul. Mater. Sci. Eng. **17**, 084002 (2009); R. M. Nieminen, *ibid.* **17**, 084001 (2009); W. R. L. Lambrecht, Phys. Status Solidi B **248**, 1547 (2011).

[21] J. B. Goodenough and Y. Kim, Chem. Mater. **22**, 587 (2010).

[22] F. J. Owens, Phys. E (Amsterdam) **25**, 404 (2005).

[23] A. K. Agrawal and S. A. Jenekhe, Chem. Mater. **8**, 579 (1996).

[24] K. Seki, T. Furuyama, T. Kawasumi, Y. Sakurai, H. Ishii, K. Kajikawa, Y. Ouchi, and T. Masuda, J. Phys. Chem. B **101**, 9165 (1997).

[25] M. K. Y. Chan and G. Ceder, Phys. Rev. Lett. **105**, 196403 (2010).

[26] C. R. Fincher Jr., M. Ozaki, M. Tanaka, D. Peebles, L. Lauchlan, A. J. Heeger, and A. G. MacDiarmid, Phys. Rev. B **20**, 1589 (1979).

[27] G. Leising, Phys. Rev. B **38**, 10313 (1988).

[28] S. Rohra, E. Engel, and A. Görling, Phys. Rev. B **74**, 045119 (2006).

[29] K. Oyaizu, T. Sukegawa, and H. Nishide, Chem. Lett. **40**, 184 (2011).

[30] K. Oyaizu and H. Nishide, Adv. Mater. **21**, 2339 (2009).

[31] J. W. Mintmire and C. T. White, Phys. Rev. B **35**, 4180 (1987).

[32] E. J. Bylaska, J. H. Weare, and R. Kawai, Phys. Rev. B **58**, R7488 (1998).

[33] G. Sun, J. Kürti, M. Kertesz, and R. H. Baughman, J. Chem. Phys. **117**, 7691 (2002).

[34] H. Lee, W. I. Choi, M. C. Nguyen, M.-H. Cha, E. Moon, and J. Ihm, Phys. Rev. B **76**, 195110 (2007).

[35] P. Sony, A. Shukla, and C. Ambrosch-Draxl, Phys. Rev. B **82**, 035213 (2010).

[36] C. S. Yannoni and T. C. Clarke, Phys. Rev. Lett. **51**, 1191 (1983).

[37] C. H. Choi, M. Kertesz, and A. Karpfen, J. Chem. Phys. **107**, 6712 (1997).

[38] S. Hirata, H. Torii, and M. Tasumi, Phys. Rev. B **57**, 11994 (1998).

[39] J. L. Brédas, J. Chem. Phys. **82**, 3808 (1985).

[40] J. P. Perdew and M. Levy, Phys. Rev. Lett. **51**, 1884 (1983).

[41] L. J. Sham and M. Schlüter, Phys. Rev. Lett. **51**, 1888 (1983).

[42] P. Mori-Sánchez, A. J. Cohen, and W. Yang, Phys. Rev. Lett. **100**, 146401 (2008); A. J. Cohen, P. Mori-Sánchez, and W. Yang, Phys. Rev. B **77**, 115123 (2008).